Heterometal-Embedded Organic Conjugate Frameworks from Alternating Monomeric Iron and Cobalt Metalloporphyrins and Their Application in Design of Porous Carbon Catalysts

Qipu Lin, Xianhui Bu, Aiguo Kong, Chengyu Mao, Fei Bu, and Pingyun Feng**

Porous covalent networks (PCNs), also known in various forms as covalent organic frameworks (COFs),[1] conjugated microporous polymers (CMPs),[2] porous aromatic frameworks (PAFs), etc.,[3] are gaining increasing interest. Some attractive properties of PCNs are well-defined chemical composition and intermonomer connectivity of various dimensions, lightweight, permanent porosity, high thermal/chemical stability, and versatility in molecular design.[1d] So far, PCNs are generally metal-free or homometallic,[4] and few heterometallic combinations are known, which limits the applications of PCNs in areas where heterometallic compositions could provide unique synergistic advantages.[5]

In comparison, heterometallic metal–organic framework (MOFs) are well known, many of which were synthesized from heterofunctional ligands.[6] Examples include different types of metalloligands such as metalloporphyrin,[6b] organometallic,[6d] dipyrrinato,[6e] salen,[6f,g] or tris(dipyrrinato)[6h] complexes, and trigonal prismatic cluster $[Cr_3O(isonic)_6(H_2O)_3]^+$ (isonic = isonicotinate).[7] Such preformed synthons use peripheral donor atoms to coordinate with the secondary metal ions/clusters for the framework formation. Other strategies for creating heterometallic MOFs include charge balance/offset, extended hook, and postsynthetic metalation.[8] In general, the crystallographic ordering of heterometals results from their complementary coordination properties. For those with the similar coordination preference, the targeted design and synthesis of PCNs or MOFs with controlled distribution of heterometals remains challenging.

Our interest in heterometallic systems stems from a desire to fabricate alternative electrode materials for oxygen reduction reaction (ORR), due to the scarcity of Pt.[5b,9] It has been demonstrated that the Fe&Co dual-doped N–M–C compositions (M denotes transition metal) are among the most promising systems for the development of high-performance electrocatalysts.[10] The bimetallic catalysts with both Fe and Co can benefit simultaneously from the unique graphene-rich morphology, enhanced corrosion resistance due to the presence of cobalt, and the intrinsically active FeN_x sites, as shown by the earlier studies such as FeCo-EDA/C (EDA = ethylenediamine) by Choi et al.,[10a] FeCo-PANI/C (PANI = polyaniline) by Wu et al.,[10b] FeCo-OMPC (OMPC = ordered mesoporous porphyrinic carbons) by Cheon et al.,[10c] and FeCo-MFR/C (MFR = melamine-formaldehyde resin) by Zhao et al.[10d]

So far the existing methods for fabricating N–FeCo–C hybrids typically involve mixing of the sources of nitrogen, carbon, and transition metals (Fe and Co), followed by thermal treatment. In these procedures, Fe and Co precursors as well as the N source are generally dispersed disorderly on or mixed randomly with the carbon supports, which makes it hard to achieve the ordering of the active electrocatalytic moieties.[5b] We anticipate that the precise control of the Fe and Co fragments in the predesigned precursors with rigid frameworks could help to retain to a substantial degree both the original porosity and relative locations of heteroatom sites in the resulting carbonized materials, which would serve as a powerful method for the creation of high-performance ORR catalysts.

Here, we report on a rational design and artful synthesis of a new family of non-precious metal catalysts termed heterometalloporphyrinic porous carbons. With preintegrated compositional and structural features, these new materials exhibit Pt-like catalytic activity for ORR in both alkaline and acidic media. Our synthetic strategy has several advantages. First, unlike random blending and nanocasting different Fe and/or Co complexes onto supports, the materials made here were prepared from the extended covalent network in which Fe- and Co-containing porphyrinic monomers are alternately distributed. Such ordered distribution of Fe and Co precursors represents our unique strategy to approach the homogeneity of active components in the final catalysts. Second, the pore volume can be tuned by taking advantage of diverse types of monomers with different geometric features, and the resulting hierarchical porosity should aid efficient transport of the fuel molecules. Third, the conjugated interconnection in precursors is quite tolerant of harsh heat treatment, which helps to retain the high active porphyrin-like moieties for ORR during carbonization. Indeed, the ORR activity reported here is among the best non-precious metal catalysts known so far.[11]

Dr. Q. Lin, Dr. A. Kong, C. Mao, F. Bu, Prof. P. Feng
Department of Chemistry
University of California
Riverside, CA 92521, USA
E-mail: pingyun.feng@ucr.edu
Prof. X. Bu
Department of Chemistry and Biochemistry
California State University
Long Beach, CA 90840, USA
E-mail: xianhui.bu@csulb.edu

DOI: 10.1002/adma.201500727

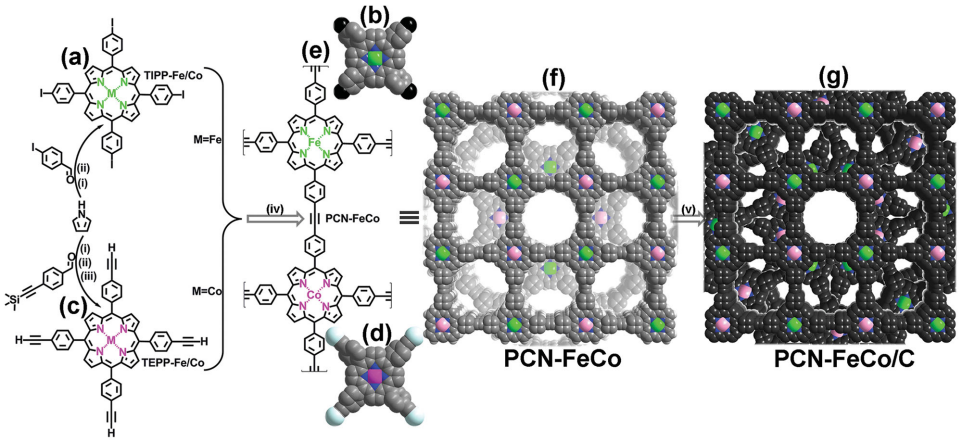

Figure 1. Schematic diagram of the synthesis of a,b) TIPP-M and c,d) TEPP-M (M = Fe, Co) monomers, e,f) porphyrinic conjugated network PCN-FeCo, and g) carbonization product PCN-FeCo/C. (FeFe/C and CoCo/C are prepared by the same synthetic route.) Reagents and conditions: i) propionic acid, reflux, 3 h; ii) $Co(OAc)_2{\cdot}4H_2O$ or $FeCl_2{\cdot}4H_2O$, $CHCl_3$-CH_3OH, reflux, 12 h; iii) tetrabutylammonium fluoride (TBAF), THF-CH_2Cl_2, r.t., 1 h; iv) $Pd_2(dba)_3$, $AsPh_3$, THF/Et_3N, 50 °C, 72 h. TIPP = 5,10,15,20-tetrakis(4-iodophenyl)porphyrin and TEPP = 5,10,15,20-tetrakis(4-ethynylphenyl)porphyrin.

Shown in **Figure 1** is the schematic diagram describing the multistep synthesis of heterometal catalyst based on alternately conjugated networking method. Two types of porphyrinic monomers with different peripheral functionalities were first made through the porphyrin synthesis, followed by metallization with Fe or Co. Sonagashira–Hagihara coupling reactions using such preformed metalloporphyrin monomers (with a stoichiometric ratio of 1:1) were devised. Three possible combinations could be realized, resulting in a series of metallic-constituent-controllable metallo-multiporphyrin porous conjugated networks, designated as PCN-MM (MM = FeCo, FeFe, CoCo). Subsequent carbonization was performed to convert the porous and robust polymers into heterometalloporphyrinic carbons (details are provided in the Supporting Information).

We next conduct extensive physicochemical characterization on heterometalloporphyrinic PCN-FeCo and its carbonized product PCN-FeCo/C (800 °C was identified as the optimum annealing temperature). Solid-state ^{13}C NMR spectrum (**Figure 2**a) of the acid-washed PCN-FeCo polymer shows four broad peaks at 149.65, 140.52, 130.23, and 120.53 ppm assignable to the phenylene moiety and porphyrin macrocycle,[2b] and the weak resonance peak at 91.60 ppm is attributed to the acetylene group.[12] The solid-state UV–vis diffuse reflectance spectrum of the PCN-FeCo shows the characteristic peaks relative to the Soret- and Q-bands of the porphyrins.[13] The efficiency of network formation can be demonstrated by the high yield obtained after purification (>95% yield) and further supported by elemental analysis (C,H,N), thermogravimetric analysis (TGA), energy dispersive X-ray (EDX), inductively coupled plasma-mass spectroscopy (ICP-MS), and Fourier transform infrared (FTIR) spectra (provided in the Supporting Information).

During the heat treatment under argon, PCN-FeCo formed graphitic carbon structure, according to powder X-ray diffraction (PXRD). The formation of graphene sheets appears to be closely associated with the improved durability of the final catalyst.[9a] The morphology of the ORR-active PCN-FeCo/C is shown by the scanning electron microscopy (SEM) images in Figure 2b. Elemental mapping with EDX imaging (Figure S21, Supporting Information) reveals that the iron, cobalt, and nitrogen species are homogeneously distributed throughout the structure. Presumably due to the strong network bonding, the sheet-like structure in PCN-FeCo could be retained after carbonization. Transmission electron microscopy (TEM) and its high-resolution TEM images of the PCN-FeCo/C (Figure S22, Supporting Information) show the presence of onion-like graphitic nanoshells together with somewhat metal aggregate particles,[10b] verified by the diffraction rings/spots in the selected area electron diffraction (SAED) pattern (Figure S23, Supporting Information). Such a well-defined graphitic carbon shell was correlated to an increase in the catalytic properties, especially performance durability in O_2-saturated solution.[9a] In addition, solid-state diffuse reflectance spectroscopy (Figure 2c) indicates that the pyrolytic product did retain some porphyrinic characteristics.

EDX and elemental analyses were performed to probe the chemical composition of the carbon composite of PCN-FeCo/C (provided in the Supporting Information). The C, H, N, Fe, and Co contents were determined to be 69.89, 1.03, 4.74, 1.4, and 1.3 wt%, respectively. Because the surface chemistry is of particular interest for catalytic applications, the electronic states of C, N, Fe, and Co were examined by X-ray photoelectron spectroscopy (XPS) measurements. As shown in Figure 2d, the high-resolution N 1s spectrum is deconvoluted into three peaks at 398.5, 399.6, and 400.8 eV, corresponding to pyridinic, metal-coordinated, and graphitic nitrogen species, respectively.[11a,14] High-resolution Fe 2p and Co 2p XPS spectra are given in Figures S28 and S29 (Supporting Information), respectively. The position for $3p_{3/2}$ peak at 710.8 eV matches well with that for Fe, while one dominant peak at 780.6 eV, assigned to $3p_{3/2}$ for Co was also observed. Such binding energy of the peaks provides evidence supporting the formation of FeN_x and/or CoN_x.[11b,15] In addition, the C 1s peak for the PCN-FeCo/C was centered at 284.9 eV (graphitic carbon), and was slightly asymmetric, which is a common characteristic for N-doped carbon materials.[11c]

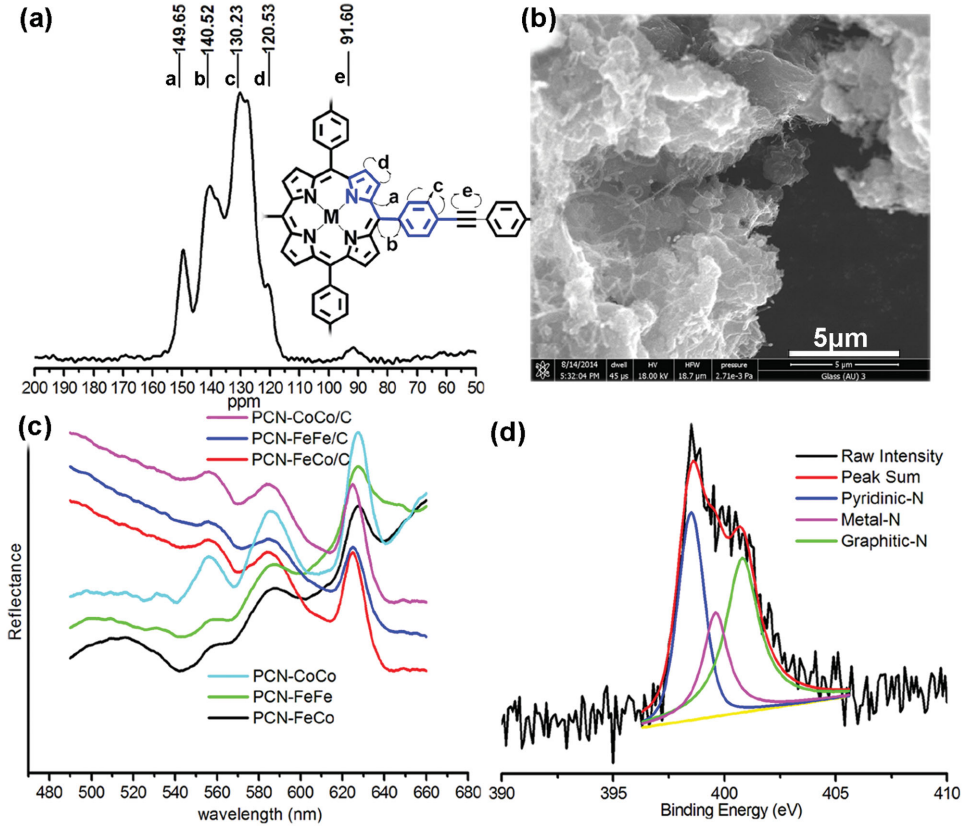

Figure 2. a) Solid-state ^{13}C NMR spectrum of the PCN-FeCo. b) SEM image of the PCN-FeCo/C. c) UV–vis diffuse reflectance spectra of the PCNs and their carbonization products. d) XPS N 1s spectra of the PCN-FeCo/C.

To gain insight into the pore properties of PCN-FeCo/C, we measured the N_2 adsorption–desorption isotherms at 77 K (**Figure 3**a). The isotherm showed atypical type-I behavior, with a steep increase at low pressure and the slight hysteretic trait of the desorption isotherm at high pressure, suggesting the presence of hierarchical micromesopores. The surface area for PCN-FeCo/C (930 $m^2\ g^{-1}$) is only slightly decreased compared to that of precursor PCN-FeCo (1260 $m^2\ g^{-1}$), as determined using Brunauer–Emmet–Teller technique. The pore size distribution was centered at 0.9 and 3.9 nm, as determined from the adsorption isotherm using the Horvath–Kawazoe and desorption isotherm using the Barrett–Joyner–Halenda model, respectively (Figure S34, Supporting Information).

The pore properties were further examined by measuring CO_2 isotherms of PCN-FeCo and PCN-FeCo/C (Figure 3b). The data gave the CO_2 uptakes of 71.3 and 46.1 $cm^3\ g^{-1}$ at 273 and 298 K, respectively, for the carbonization product (PCN-FeCo/C) at ambient pressure, which are only slightly lower than that of PCN-FeCo (78.4 and 47.3 $cm^3\ g^{-1}$). To determine the strength of the interactions between CO_2 and the carbon matrix, the isosteric heat of adsorption (Q_{st}) for the PCN-FeCo/C was calculated from the CO_2 isotherms measured at 273 and 298 K, to be up to 36.7 kJ mol^{-1} at zero coverage, much higher than that of PCN-FeCo (27.5 kJ mol^{-1}), reflecting the greater affinity between metalloporphyrinic carbon host with CO_2. We have also evaluated their acetylene (C_2H_2) and methane (CH_4) sorption properties and observed high selectivity toward C_2H_2 over CH_4 for both PCN-FeCo (Figure S32, Supporting Information) and PCN-FeCo/C (Figure S35, Supporting Information).

To evaluate the electrocatalytic activities for ORR, we first carried out cyclic voltammetry (CV) measurements on these newly synthesized PCN/C samples in 0.1 M KOH solution (**Figure 4**a). In an argon-saturated solution, the CV curves within the entire potential range showed virtually featureless slopes for the cathodic current. In contrast, the well-defined cathodic peaks appeared in all the CV curves of the three samples in the solution saturated with O_2. Compared with the pure cobalt-containing sample of PCN-CoCo/C (peak potential of ≈0.83 V versus the reversible hydrogen electrode, RHE, the same below), the Fe-incorporated PCN-FeFe/C showed much more positive ORR potentials (0.86 V). In particular, the peak potential of Fe&Co dual-doped electrode (PCN-FeCo/C) reached 0.88 V.

To gain further insight into the ORR process for the electrodes, rotating-disk electrode (RDE) measurements were performed in O_2-saturated KOH–H_2O electrolyte at a scan rate of 10 mV s^{-1} (Figure 4b). For comparison, the 20 wt% Pt/C (Alfa) reference catalyst was also examined. It was determined that the PCN-FeCo/C displayed a more positive onset potential (1.00 V) than that of PCN-FeFe/C (0.97 V), and PCN-CoCo/C (0.92 V). Furthermore, the heterometallic product afforded a half-wave potential of 0.85 V, comparable to that of Pt/C (0.84 V). The PCN-FeCo/C showed a highly stable diffusion-limiting current, which was superior to the monometallic counterparts, and even

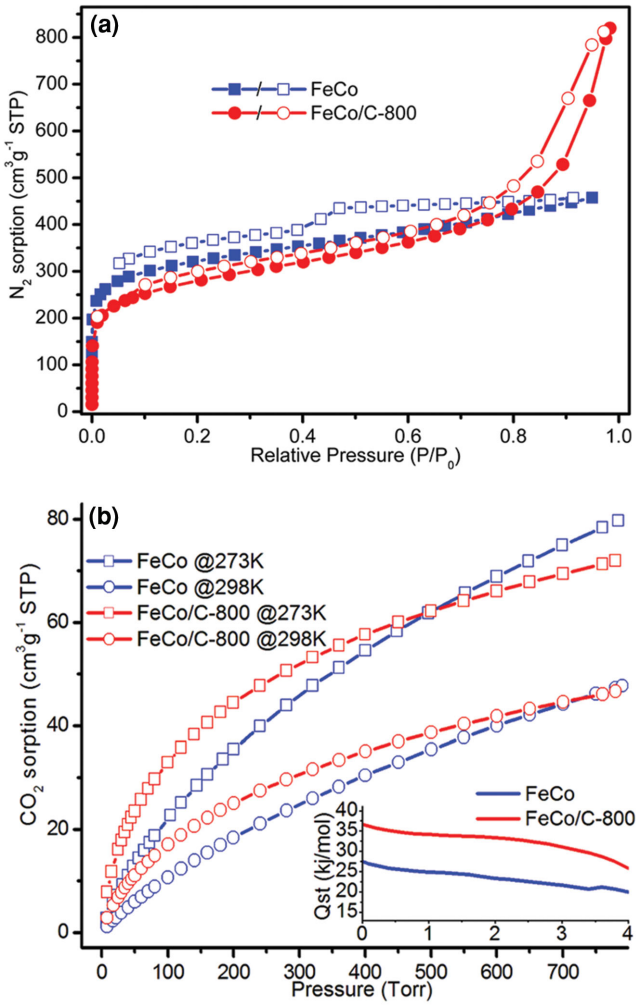

Figure 3. a) N_2 adsorption–desorption curves of PCN-FeCo and PCN-FeCo/C. b) CO_2 adsorption isotherms of PCN-FeCo and PCN-FeCo/C at 273 and 298 K, respectively (inset: isosteric heat of adsorption, Q_{st}).

comparable to Pt/C. The results are in agreement with the CV observations, and further confirm that the heterometal-doped materials can significantly enhance the ORR activity.

Subsequently, Koutecky–Levich (K–L) equations were used to determine catalytic reaction pathway. On the basis of RDE polarization curves at different rotation rates, the electron transfer number (n) of PCN-FeCo/C was calculated to be 4.2 ± 0.1 at 0.1–0.6 V (Figure 4d), suggesting a mainly 4e oxygen reduction process. To investigate the methanol crossover effects and durability, we carried out chronoamperometric measurements. As shown in Figure S44 (Supporting Information), all of the PCN/C electrodes exhibited a remarkably better long-term stability than the commercial Pt/C catalyst. Moreover, it was found that the PCN-FeCo/C was almost free from the methanol crossover effect.

Finally, we investigated the ORR performance of PCN-derived electrodes, along with Pt/C reference catalyst, in 0.1 M $HClO_4$ media. As shown in Figure S41 (Supporting Information), the Fe-containing PCN-FeFe/C and PCN-FeCo/C electrodes showed much higher peak potential (by a shift of 26 and 34 mV, respectively), compared to that of cobalt-only-doped PCN-CoCo/C. As further determined by RDE experiments and relative to the Fe-free product, a significant improvement in activity is also observed with the PCN-FeFe/C sample, as evidenced by positive shifts in onset (from 0.85 to 0.88 V) and half-wave $E_{1/2}$ (from 0.71 to 0.74 V) potentials. Again, the binary catalyst PCN-FeCo/C was found to give the highest activity, i.e., the most positive onset (0.90 V) and $E_{1/2}$ (0.76 V) potentials. The ORR polarization curve of the PCN-FeCo/C catalyst in 0.1 M $HClO_4$ was nearly identical to that of the Pt/C catalyst. For electrode of PCN-FeCo/C, the K–L plots at various potentials also exhibit good linearity and parallelism, indicating first-order reaction kinetics for ORR with respect to the concentration of dissolved O_2. The electron transfer number (n) was calculated to be 4.2 ± 0.1 at 0.1–0.6 V from the slopes of K–L plots, suggesting that it favors a 4e oxygen reduction process as well, similar to that by Pt/C.

For the sustainable use of fuel cell electrocatalysts, their long-term durability is critical.[5b,9b] In addition to high activity, the PCN-derived nanocomposites also exhibit high stability. The chronoamperometric plots for the PCN/C catalysts are shown in Figure 4f. Among them, the current density of PCN-FeCo/C declines by only 10% after 14 h, indicating much greater durability in acidic solution than Pt/C. We next examined its tolerance against poisoning with fuel molecules, which is directly relevant to its potential use in alcohol fuel cells. The ORR polarization curve of the PCN-FeCo/C in the presence of 0.5 M methanol exhibited only a small shift of half-wave potential (30 mV), while the Pt/C catalyst showed much more negative shift (300 mV). Such excellent performance stability can be attributed to the highly graphited nanostructures.[9a]

Direct carbonization of heterometallo precursors in the form of porous conjugated frameworks has the unique advantages for creating hierarchical porosity and ordered distribution of catalytically active porphyrin-like segments in the final material. The combined use of complementary metal centers (Fe and Co in this work) provides for synergistic effect, leading to novel materials with both high ORR activity and durability. Although the exact contributions to the catalytic behavior by the Fe and Co species are not well understood, it was hypothesized that the role of Fe could be attributable to the formation of the intrinsically active metal–N_x sites which contribute to the ORR performance,[10b,11c] while the performance durability may be due to the high graphitization of carbon structures (partially derived from Co) which serve as a robust matrix for hosting active sites to increase the resistance to oxidative attack.[11a,b] In addition, it was also suggested that changes in the charge and spin densities of the carbon lattice[16] (variations in the nanoscale work functions)[17] could be significant factors for the superior performance observed with multiple-dopants-incorporated nanocarbons. These effects and high surface area of PCN-FeCo/C appear responsible for its significantly high electrocatalytic performance.

In conclusion, we have demonstrated the use of alternately conjugated networking method to prepare highly porous heterometalloporphyrin materials of PCN-FeCo, which is the first example of heterometallic porous covalent solids with ordered alternation of iron and cobalt chelate complexes. Its subsequent

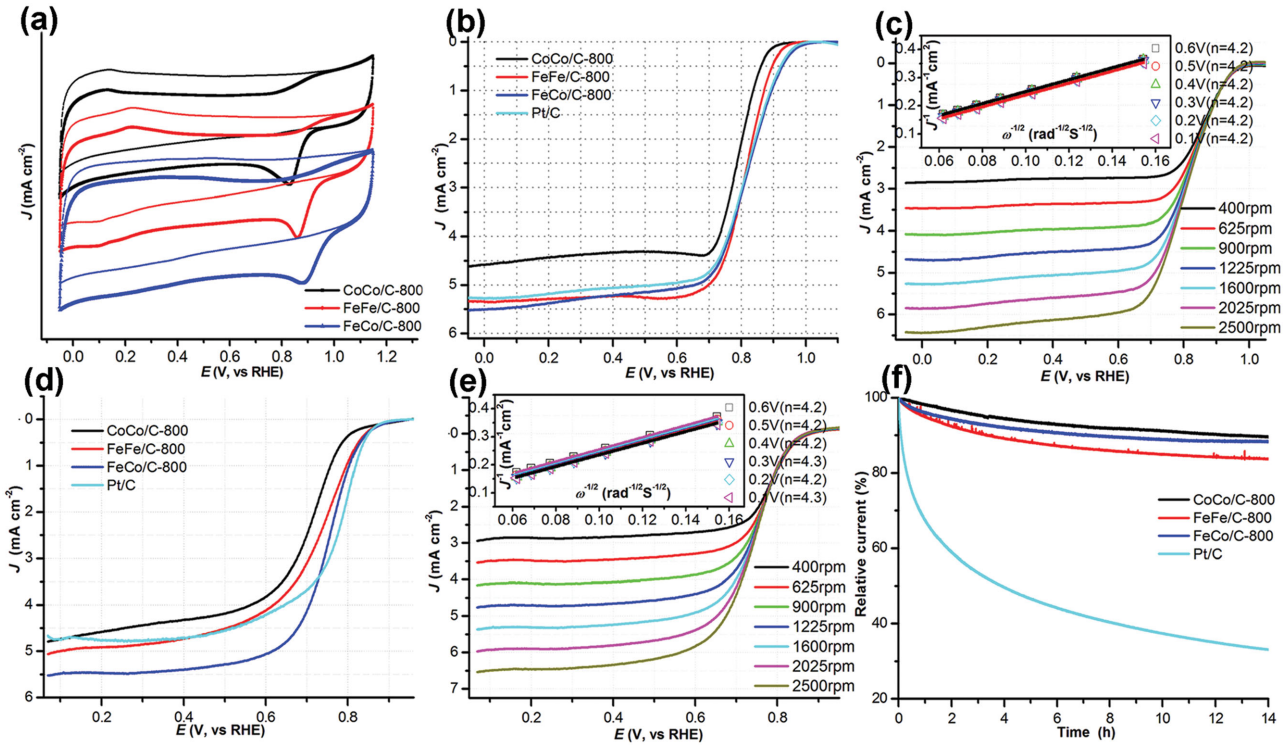

Figure 4. a) CV and b) RDE polarization curves (at rotation rate of 1600 rpm) on PCN/C and 20% Pt/C (Alfa) in 0.1 M KOH solution. c) RDE polarization curves on PCN-FeCo/C at different rotation rates, inset: K–L plot of J^{-1} versus ω^{-1}. d) RDE polarization curves at 1600 rpm on PCN/C and 20% Pt/C in 0.1 M $HClO_4$ solution. e) RDE polarization curves on PCN-FeCo/C at different rotation rates, inset: K–L plot of J^{-1} versus ω^{-1}. f) Current versus time (i–t) chronoamperometric response of the PCN/C and Pt/C at 0.5 V (vs RHE) in O_2-saturated 0.1 M $HClO_4$ at 1600 rpm, respectively.

carbonization gives rise to Fe and Co co-doped azotized-carbon composite of PCN-FeCo/C. The newly synthesized catalyst exhibits very high ORR activity and remarkable electrochemical stability in both alkaline and acidic electrolyte and compares favorably to the benchmark Pt/C. The prominent performance of the PCN-FeCo/C can be attributed to its advanced features including large surface area, substantial graphitization, high density of uniformly distributed heterometallic active moieties. Significantly, we point out that the design concept presented here to prepare heterometal catalysts is general and applicable to other systems as well.

Experimental Section

Typical Synthesis of PCN-FeCo/C: Atropurpureus powder of PCN-FeCo was obtained in ≈97% yield by reacting 5,10,15,20-tetrakis(4-iodophenyl)-porphyrin-iron (TIPP-Fe, 1.0 mmol) and 5,10,15,20-tetrakis(4-ethynylphenyl)porphyrin-cobalt (TEPP-Co, 1.0 mmol) in a mixed solvent of anhydrous THF:Et_3N (80 mL:20 mL) in the presence of catalyst tris(dibenzylideneacetone)dipalladium(0) ($Pd_2(dba)_3$, 0.05 mmol) plus triphenylarsine ($AsPh_3$, 2.0 mmol), under argon atmosphere and at 50 °C. The mixture was stirred for 72 h. Once completed, the precipitate was washed by Soxhlet extraction to remove the residues. The resulting solid was immersed in pyridine for 12 h, subsequently filtered off and heated in tube furnace under argon atmosphere at a heating rate of 3 °C min^{-1} up to preset temperature for 4 h. The synthesis of porphyrin monomers and PCN-FeFe/C and PCN-CoCo/C are provided in the Supporting Information.

Supporting Information

Supporting Information is available from the Wiley Online Library or from the author.

Acknowledgements

The research was supported by the U.S. Department of Energy, Office of Basic Energy Sciences, Division of Materials Sciences and Engineering under Award No. DE-FG02-13ER46972.

Received: February 11, 2015
Revised: March 15, 2015
Published online: April 27, 2015

[1] a) A. P. Cote, A. I. Benin, N. W. Ockwig, M. O'Keeffe, A. J. Matzger, O. M. Yaghi, *Science* **2005**, *310*, 1166; b) E. L. Spitler, W. R. Dichtel, *Nat. Chem.* **2010**, *2*, 672; c) A. M. Shultz, O. K. Farha, J. T. Hupp, S. T. Nguyen, *Chem. Sci.* **2011**, *2*, 686; d) X. Feng, X. Ding, D. Jiang, *Chem. Soc. Rev.* **2012**, *41*, 6010; e) D. Beaudoin, T. Maris, J. D. Wuest, *Nat. Chem.* **2013**, *5*, 830; f) G. H. Bertrand, V. K. Michaelis, T. C. Ong, R. G. Griffin, M. Dinca, *Proc. Natl. Acad. Sci. USA* **2013**, *110*, 4923; g) S. Y. Ding, W. Wang, *Chem. Soc. Rev.* **2013**, *42*, 548.
[2] a) A. I. Cooper, *Adv. Mater.* **2009**, *21*, 1291; b) L. Chen, Y. Yang, D. L. Jiang, *J. Am. Chem. Soc.* **2010**, *132*, 9138.
[3] a) T. Ben, H. Ren, S. Ma, D. Cao, J. Lan, X. Jing, W. Wang, J. Xu, F. Deng, J. M. Simmons, S. Qiu, G. Zhu, *Angew. Chem. Int. Ed.*

2009, *48*, 9457; b) W. Lu, D. Yuan, J. Sculley, D. Zhao, R. Krishna, H. C. Zhou, *J. Am. Chem. Soc.* **2011**, *133*, 18126; c) D. Yuan, W. Lu, D. Zhao, H. C. Zhou, *Adv. Mater.* **2011**, *23*, 3723; d) W. Lu, Z. Wei, D. Yuan, J. Tian, S. Fordham, H.-C. Zhou, *Chem. Mater.* **2014**, *26*, 4589.

[4] a) Z. Xie, C. Wang, K. E. deKrafft, W. Lin, *J. Am. Chem. Soc.* **2011**, *133*, 2056; b) J. W. Colson, W. R. Dichtel, *Nat. Chem.* **2013**, *5*, 453; c) K. K. Tanabe, M. S. Ferrandon, N. A. Siladke, S. J. Kraft, G. Zhang, J. Niklas, O. G. Poluektov, S. J. Lopykinski, E. E. Bunel, T. R. Krause, J. T. Miller, A. S. Hock, S. T. Nguyen, *Angew. Chem. Int. Ed.* **2014**, *53*, 12055.

[5] a) H.-L. Jiang, Q. Xu, *J. Mater. Chem.* **2011**, *21*, 13705; b) G. Wu, P. Zelenay, *Acc. Chem. Res.* **2013**, *46*, 1878.

[6] a) M. B. Zhang, J. Zhang, S. T. Zheng, G. Y. Yang, *Angew. Chem. Int. Ed.* **2005**, *44*, 1385; b) W. Y. Gao, M. Chrzanowski, S. Ma, *Chem. Soc. Rev.* **2014**, *43*, 5841; c) H. He, G. J. Cao, S. T. Zheng, G. Y. Yang, *J. Am. Chem. Soc.* **2009**, *131*, 15588; d) K. Oisaki, Q. W. Li, H. Furukawa, A. U. Czaja, O. M. Yaghi, *J. Am. Chem. Soc.* **2010**, *132*, 9262; e) J. R. Stork, V. S. Thoi, S. M. Cohen, *Inorg. Chem.* **2007**, *46*, 11213; f) C. Zhu, G. Yuan, X. Chen, Z. Yang, Y. Cui, *J. Am. Chem. Soc.* **2012**, *134*, 8058; g) Y. Liu, X. Xi, C. Ye, T. Gong, Z. Yang, Y. Cui, *Angew. Chem. Int. Ed.* **2014**, *53*, 13821; h) L. Carlucci, G. Ciani, S. Maggini, D. M. Proserpio, M. Visconti, *Chem. Eur. J.* **2010**, *16*, 12328.

[7] a) A. Schoedel, L. Wojtas, S. P. Kelley, R. D. Rogers, M. Eddaoudi, M. J. Zaworotko, *Angew. Chem. Int. Ed.* **2011**, *50*, 11421; b) A. Schoedel, W. Boyette, L. Wojtas, M. Eddaoudi, M. J. Zaworotko, *J. Am. Chem. Soc.* **2013**, *135*, 14016.

[8] a) S. T. Zheng, X. Zhao, S. Lau, A. Fuhr, P. Feng, X. Bu, *J. Am. Chem. Soc.* **2013**, *135*, 10270; b) S. T. Zheng, T. Wu, F. Zuo, C. Chou, P. Feng, X. Bu, *J. Am. Chem. Soc.* **2012**, *134*, 1934; c) L. Q. Ma, J. M. Falkowski, C. Abney, W. B. Lin, *Nat. Chem.* **2010**, *2*, 838; d) J. Zhang, T. Wu, C. Zhou, S. Chen, P. Feng, X. Bu, *Angew. Chem. Int. Ed.* **2009**, *48*, 2542.

[9] a) L. M. Dai, *Acc. Chem. Res.* **2013**, *46*, 31; b) Z. Chen, D. Higgins, A. Yu, L. Zhang, J. Zhang, *Energ. Environ. Sci.* **2011**, *4*, 3167.

[10] a) J. Y. Choi, R. S. Hsu, Z. W. Chen, *J. Phys. Chem. C* **2010**, *114*, 8048; b) G. Wu, K. L. More, C. M. Johnston, P. Zelenay, *Science* **2011**, *332*, 443; c) J. Y. Cheon, T. Kim, Y. Choi, H. Y. Jeong, M. G. Kim, Y. J. Sa, J. Kim, Z. Lee, T. H. Yang, K. Kwon, O. Terasaki, G. G. Park, R. R. Adzic, S. H. Joo, *Sci. Rep.* **2013**, *3*, 2715; d) Y. Zhao, K. Watanabe, K. Hashimoto, *J. Mater. Chem. A* **2013**, *1*, 1450.

[11] a) Z. S. Wu, L. Chen, J. Liu, K. Parvez, H. Liang, J. Shu, H. Sachdev, R. Graf, X. Feng, K. Mullen, *Adv. Mater.* **2014**, *26*, 1450; b) Z. Xiang, Y. Xue, D. Cao, L. Huang, J. F. Chen, L. Dai, *Angew. Chem. Int. Ed.* **2014**, *53*, 2433; c) S. W. Yuan, J. L. Shui, L. Grabstanowicz, C. Chen, S. Commet, B. Reprogle, T. Xu, L. P. Yu, D. J. Liu, *Angew. Chem. Int. Ed.* **2013**, *52*, 8349.

[12] a) S. Fischer, J. Schmidt, P. Strauch, A. Thomas, *Angew. Chem. Int. Ed.* **2013**, *52*, 12174; b) Q. P. Lin, J. Z. Lu, Z. D. Yang, X. C. Zeng, J. Zhang, *J. Mater. Chem. A* **2014**, *2*, 14876.

[13] A. Fateeva, P. A. Chater, C. P. Ireland, A. A. Tahir, Y. Z. Khimyak, P. V. Wiper, J. R. Darwent, M. J. Rosseinsky, *Angew. Chem. Int. Ed.* **2012**, *51*, 7440.

[14] H. W. Liang, W. Wei, Z. S. Wu, X. Feng, K. Mullen, *J. Am. Chem. Soc.* **2013**, *135*, 16002.

[15] Y. Zhao, K. Watanabe, K. Hashimoto, *J. Am. Chem. Soc.* **2012**, *134*, 19528.

[16] a) K. Gong, F. Du, Z. Xia, M. Durstock, L. Dai, *Science* **2009**, *323*, 760; b) L. Yang, S. Jiang, Y. Zhao, L. Zhu, S. Chen, X. Wang, Q. Wu, J. Ma, Y. Ma, Z. Hu, *Angew. Chem. Int. Ed.* **2011**, *50*, 7132; c) I. Y. Jeon, S. Zhang, L. Zhang, H. J. Choi, J. M. Seo, Z. Xia, L. Dai, J. B. Baek, *Adv. Mater.* **2013**, *25*, 6138; d) Y. Jiao, Y. Zheng, M. Jaroniec, S. Z. Qiao, *J. Am. Chem. Soc.* **2014**, *136*, 4394; e) L. Zhang, Z. Xia, *J. Phys. Chem. C* **2011**, *115*, 11170.

[17] J. Y. Cheon, J. H. Kim, J. H. Kim, K. C. Goddeti, J. Y. Park, S. H. Joo, *J. Am. Chem. Soc.* **2014**, *136*, 8875.